

Investigation of water evolution and transport in fuel cells with high resolution synchrotron x-ray radiography

I. Manke^{a)}*Institute of Materials Science and Technology, Technical University Berlin, 10623 Berlin, Germany*

Ch. Hartnig, M. Grünerbel, and W. Lehnert

Centre for Solar Energy and Hydrogen Research, 89081 Ulm, Germany

N. Kardjilov, A. Haibel, A. Hilger, and J. Banhart

Hahn-Meitner Institute Berlin, 14109 Berlin, Germany

H. Rieseemeier

Federal Institute for Materials Research and Testing, 12205 Berlin, Germany

(Received 10 November 2006; accepted 25 March 2007; published online 23 April 2007)

The authors report on *in situ* investigations of liquid water evolution and transport in an undisturbed operating fuel cell at the microscopic level. Synchrotron x-ray radiography enhances the spatial resolution by two orders of magnitude compared to the state-of-the-art techniques in this field. The primary spots of liquid water formation, their growth, and transport inside the porous gas diffusion material were analyzed; correlations between operating conditions and the dynamics of droplet formation are described. Previous findings from modeling and simulation approaches are confirmed and the applicability for the description of *in situ* processes of a recently proposed model has been proven. © 2007 American Institute of Physics. [DOI: 10.1063/1.2731440]

In polymer electrolyte membrane (PEM) fuel cells, hydrogen and oxygen react to water; due to the separation of the anodic and cathodic processes, electric energy is produced.^{1,2} Water plays a crucial role in these fuel cells: On one hand, only the wet membrane is proton conductive; a dry polymer membrane changes its structure and the proton conductivity of the membrane breaks down. On the other hand, if the catalyst layer and the adjacent porous gas diffusion layer (GDL) are filled with liquid water, the transport of reactant and product gases (O_2 , H_2 , and H_2O) is strongly hindered and the supply of the electrochemically active area is insufficient, limiting the maximum achievable power density and affecting the lifetime of the catalysts and the GDL.^{1,2} Thus, an efficient water management providing humid conditions while simultaneously removing excess water from the cell at any operating condition is a major task and one of the key points for the efficiency and lifetime of PEM fuel cells.¹

In the past years, the interest in these issues has been steadily increasing and many advances were made.^{3–11} However, a deep insight into the fundamental processes of liquid water evolution and transport is still lacking, preventing a targeted strategy for cell development. Many studies had been focusing on theoretical modelling^{5–9} and *ex situ* investigations^{4,10} to gain some insight into the water transport processes in fuel cells. In practice, the high complexity of environmental conditions inside a fuel cell does not allow for a sufficiently detailed prediction of water evolution and transport.

Until now, there are only few techniques for *in situ* investigation. Methods requiring a special cell preparation, e.g., optically transparent components, result in an uncontrollable disturbance of the system.^{12–14} Recently, neutron radiography has been proven very useful for *in situ* investigations of water transport in the flow field channels and GDLs, but the spatial resolution (around 100 μm) is not sufficient to

visualize the formation of liquid water inside single pores of the GDL.^{15–18}

In this work, the mechanism and dynamics of liquid water formation is investigated by means of synchrotron x-ray radiography with a spatial resolution of a few micrometers which represents an increase of about two orders of magnitude compared to neutron radiography. Limitations such as low resolution or strong disturbances of the system have been overcome by this method.¹⁹ The comparatively low x-ray photon energy of 13 keV strongly enhances the sensitivity to water (avoiding the addition of a highly absorptive contrast medium) and therefore allows visualization of water despite of the x-ray absorption by the surrounding GDL material and other components.

A single cell setup as shown in Fig. 1(a) has been used for all measurements. Threefold anodic and cathodic serpentine flow fields with 1 mm wide channels and ribs and an active area of 100 cm^2 were machined in separate blank graphite composite plates (SGL Carbon) with the cooling water channels grafted in the cathodic part. Gore PRIMEA 5620 membrane electrode assemblies with a platinum loading of 0.3 mg/cm^2 on the anode and 0.4 mg/cm^2 on the cathode side were employed. A carbon fiber material (SGL

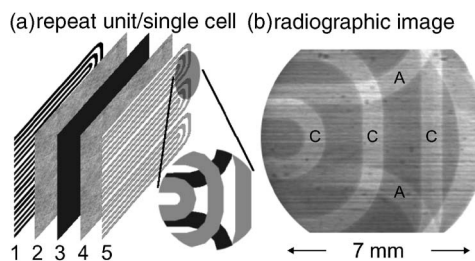


FIG. 1. (a) Scheme of the fuel cell system: (1) anodic flow field, (2) anodic gas diffusion layer, (3) catalyst coated polymer electrolyte membrane (PEM), (4) cathodic gas diffusion layer, and (5) cathodic flow field. (b) Radiograph of the part of the fuel cell marked in (a).

^{a)}Electronic mail: manke@hmi.de

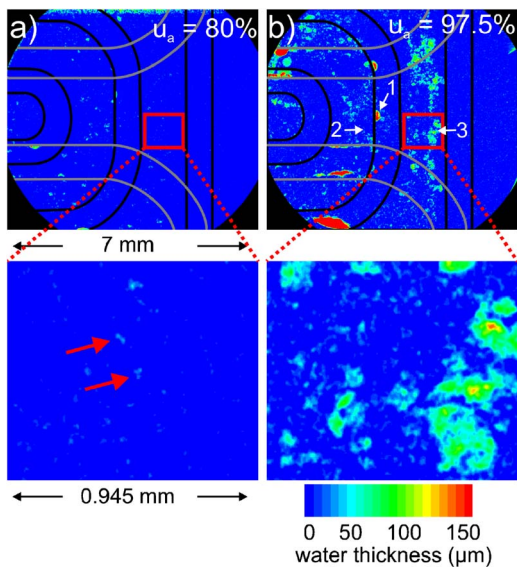


FIG. 2. (Color online) Normalized radiographs of the operating fuel cell displaying the water distribution for two different operating conditions [first row, (a) and (b)] and corresponding enlargements of the areas marked in red (second row). Flow field channels are marked by dark lines (compare to non-normalized radiograph in Fig. 1). The white arrows are referred to in Fig. 4.

Carbon 10 BB) with pore sizes typically around 20–50 μm was used as GDL; all components are optically opaque. The operating cell was investigated through small sealed holes of 8 mm diameter in the metallic end plates of the cell. The flow field and the other components remain completely unmodified. Thus the slight modification of the housing does not influence the thermal and electrical conductivity of the components and the water evolution and transport in the cell.

The experiments were performed at the tomography facility of the BAMline at the Synchrotron BESSY in Berlin (Germany). A W–Si multilayer monochromator with an energy resolution of about $\Delta E/E=10^{-2}$ was used to obtain a monochromatic 13 keV x-ray beam. A 2048 \times 2048 pixel camera (Princeton VersArray 2048B) was used to capture images up to 7 \times 7 mm² in size with the corresponding image pixel sizes between 1.5 and 3.5 μm corresponding to a physical spatial resolution of 3–7 μm . The measurement time per image was around 4.8 s, 1 s for exposure and 3.8 s for data readout.

In Fig. 1(b) a radiographic image of a cell section is displayed. The flow field channels on the anode (A) and cathode (C) side can be identified as bright structures.

The amount of liquid water produced in the cell strongly depends on the electric output current density i_0 and the so called utilization rates (fraction of total gas input which is consumed in the cell) at the anode u_A (hydrogen) and cathode u_C (aerial oxygen). The water distributions for two different operating conditions are displayed in Fig. 2 together with the corresponding enlargements of the areas marked in red. The water distribution was visualized by normalizing all images with respect to an image of the dry cell. The water thickness was quantified by means of the attenuation coefficient of water at the used x-ray energies. A homogenous water humidification background depending on operating conditions was subtracted from each image (see below).

Under the so-called dry conditions [Fig. 2(a): $u_C=25\%$, $u_A=80\%$, and $i_0=300 \text{ mA/cm}^2$] only some small water clusters of about 10–20 μm in diameter (some marked by red

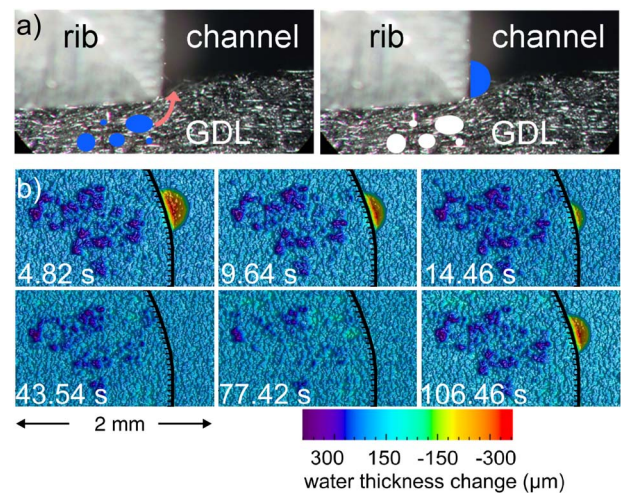


FIG. 3. (Color online) Eruptive water ejection from the gas diffusion layer (GDL) to the cathodic flow field channel. (a) Schematic illustration of the process: water (blue) inside the pores of the cathodic GDL is ejected into the flow field channel; (b) radiographs that were normalized to the image directly before eruption (not shown here). Dark blue and purple areas represent reduced amounts of water in the GDL pores while other colors indicate an increased water level, i.e., the first image (top left) shows the changes after the first 4.82 s. Within this time the pores are emptied and the water moves into the channel where it forms a droplet at the wall side (the channel has been marked by a black curved line). After some time the water droplet evaporates and the pores are filled again (i.e., the blue areas disappear) until a new ejection takes place.

arrows) containing a few picoliters were visible (located in the GDL pores) indicating that most water was transported as vapor.

In contrast, at high anodic utilization rate and output current ($u_A=97.5\%$, $i_0=500 \text{ mA/cm}^2$) many water clusters of up to 300 μm in diameter, each containing up to several hundred or thousand picoliters of water, were observed [Fig. 2(b)]. Increased utilization rates are realized by reducing gas flow leading to a decreased water transport out of the cell. The water filled pores are preferably located in the cathodic gas diffusion layer as determined from the position of the flow field ribs. The spots of liquid water are located below the central area of the ribs in between the channels. The mode of water transport varies between different locations in the cell. An eruptive transport mechanism was observed at some spots while a continuous flow of water is expected at others. Here we speak of *eruptive transport* whenever many droplets of liquid water in the gas diffusion layers are ejected into the channel and merge there into a single drop within a short period (far less than 5 s), as shown schematically in Fig. 3(a). The top left image in Fig. 3(b) shows the difference (mathematically the ratio) between the radiographs directly before and after ejection. Dark blue are the locations in the GDL where the water was first registered and values from green to red depict the places where the water moved to, i.e., the water drop formed in the channel. The complete ejection process takes place within the time difference between the two images (4.8 s). The following images were normalized in the same way and show the slow refilling of the emptied pores and the evaporation of the droplet within 10–15 s to the unsaturated gas stream at the chosen position in the flow field. After about 100 s the pores are filled again before the next eruption occurs. The behavior is periodic with an almost constant frequency and always takes place in approximately the same pores of the GDL.

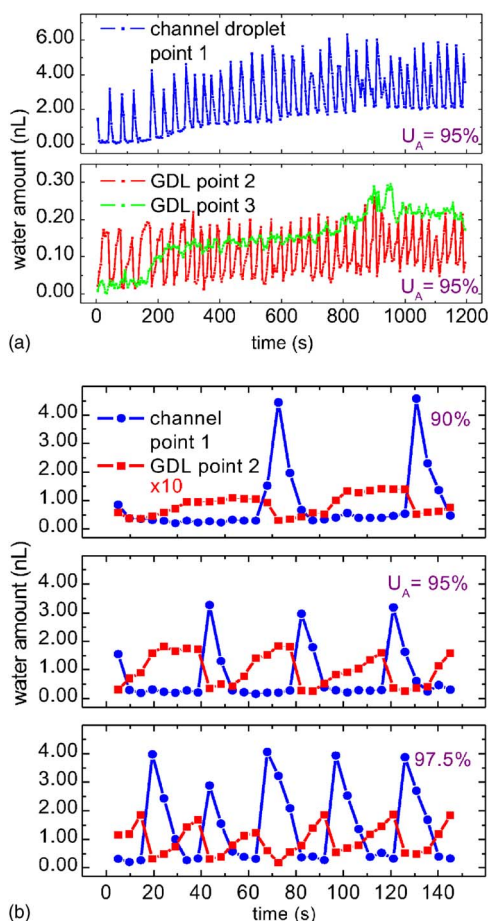


FIG. 4. (Color online) (a) Time dependence of the water amount at the three locations marked in Fig. 2(b): The water droplet in the channel at location 1 (blue) and the two locations 2 (red) and 3 (green) in the GDL. (b) Time dependence of the water amount at locations 1 (blue) and 2 (red) for three different utilization rates u_A during operation.

A quantitative analysis of water development was carried out at the three locations marked by arrows and numbers in Fig. 2(b). In Fig. 4(a), the time dependence of the pore filling level is given. The blue line shows the water quantity in a square of about $210 \times 140 \mu\text{m}^2$ around the water droplet in the channel [location 1 in Fig. 2(c)], the red line shows the water amount in an area of $35 \times 35 \mu\text{m}^2$ around a nearby water filled pore [location 2 in Fig. 2(c)]; both show a cyclic behavior with the same periodicity. A different behavior is observed at location 3 in Fig. 2(b). The pores fill gradually until a certain level is reached [green line in Fig. 4(a)], indicating a dynamic equilibrium with the gas phase. Although the amount of water remains almost constant [Fig. 4(a)], water might be transported at these spots via continuous flow.

The correlation between water droplets in the channel or water clusters in the GDL and the operating conditions of the cell is illustrated by the amount of water measured at locations 1 and 2 of Fig. 2(b) for three different operating conditions as a function of time [Fig. 4(b)]. The overall scheme is almost independent of the operating conditions, i.e., the emptying of the pores is correlated with the development of the droplet. At higher utilization rates (reduced transport of water out of the cell) the repetition time is much higher, i.e., for $u_A = 90\%$, 95% , and 97.5% the corresponding repetition times are 65 ± 5 , 40 ± 5 , and 26 ± 5 s, pointing towards an increased contribution of water transport through liquid phase.

The first appearance of liquid water droplets under the channels (Fig. 1) is in good agreement with the predictions from simulations as given, e.g., by Kulikovskiy *et al.* that are now confirmed for the water evolution at a very early stage.²⁰ The continuous GDL pore filling (Figs. 2 and 4, location 3) indicates a continuous “capillary-tree-like” transport behavior as predicted by Pasaogullari and Wang.⁵ In addition to this behavior, the eruptive transport process observed at location 2 (Figs. 2 and 4) plays a non-negligible role. Especially at high current densities this transport mechanism could be held responsible for a significant part of the water transport. Recent *ex situ* experiments by Litster *et al.*¹⁰ confirm this mechanism meaning in turn that the application of the capillary tree model as proposed in the past has to be considered carefully.

In conclusion, synchrotron x-ray radiography proved to be an invaluable tool for *in situ* investigations of operating fuel cells, yielding insights into water evolution, water transport processes, and multiphase effects. Several theoretical models and other *ex-situ* studies could be confirmed. However, *in situ* observations of primary clusters of liquid water development at the microscopic level help to verify results from numerous modeling studies and to develop new models which, on the other hand, will directly influence the development of new materials and components for fuel cells.

The authors would like to thank B. R. Müller, T. Wolk, S. Zabler, and A. Rack for help with the experiments, and J. Scholta for discussing experimental results. This project was cofinanced by the European Union and the City State of Berlin (EFRE 2000 2006 2/16).

¹C. Y. Wang, *Handbook of Fuel Cells: Fundamentals, Technology and Applications* (Wiley, Chichester, 2003), Vol. 3, pp. 337–347.

²L. Carrette, K. A. Friedrich, and U. Stimming, *Mater. Today* **1**, 5 (2001).

³M. M. Mench, Q. L. Dong, and C. Y. Wang, *J. Power Sources* **124**, 90 (2003).

⁴R. Eckl, W. Zehner, C. Leu, and U. Wagner, *J. Power Sources* **138**, 137 (2004).

⁵U. Pasaogullari and C. Y. Wang, *J. Electrochem. Soc.* **152**, 380 (2005).

⁶G. Lin, W. He, and T. Van Nguyen, *J. Electrochem. Soc.* **151**, 1999 (2004).

⁷C. Ziegler, H. M. Yu, and J. O. Schumacher, *J. Electrochem. Soc.* **152**, 1555 (2005).

⁸P. Berg, K. Promislow, J. St. Pierre, J. Stumper, and B. Wetton, *J. Electrochem. Soc.* **151**, 341 (2004).

⁹J. H. Nam and M. Kaviany, *Int. J. Heat Mass Transfer* **46**, 4595 (2003).

¹⁰S. Litster, D. Sinton, and N. Djilali, *J. Power Sources* **154**, 95 (2006).

¹¹C. Lim and C. Y. Wang, *Electrochim. Acta* **49**, 4149 (2004).

¹²X. G. Yang, F. Y. Zhang, A. L. Lubawy, and C. Y. Wang, *Electrochem. Solid-State Lett.* **7**, 408 (2004).

¹³K. Tüber, D. Pócza and C. Hebling, *J. Power Sources* **124**, 403 (2003).

¹⁴F. Y. Zhang, X. G. Yang and C. Y. Wang, *J. Electrochem. Soc.* **153**, 225 (2006).

¹⁵R. J. Bellows, M. Y. Lin, M. Arif, A. K. Thompson, and D. Jacobson, *J. Electrochem. Soc.* **146**, 1099 (1999).

¹⁶R. Satija, D. L. Jacobson, M. Arif, and S. A. Werner, *J. Power Sources* **129**, 238 (2004).

¹⁷N. Pekula, K. Heller, P. A. Chuang, A. Turhan, M. M. Mench, J. S. Brenizer, and K. Ünlü, *Nucl. Instrum. Methods Phys. Res. A* **542**, 134 (2005).

¹⁸J. Zhang, D. Kramer, R. Shimoi, Y. Ono, E. Lehmann, A. Wokaun, K. Shinohara, and G. G. Scherer, *Electrochim. Acta* **51**, 2715 (2006).

¹⁹J. Baruchel, P. Cloetens, J. Härtwig, and M. Schlenker, *Third-Generation Hard X-Ray Synchrotron Radiation Sources* (Wiley, New York, 2002), pp. 181–202.

²⁰A. A. Kulikovskiy, T. Wüster, A. Egmen, and D. Stolten, *J. Electrochem. Soc.* **152**, A1290 (2005).